Effect of Mean Stress (Stress Ratio) and Aging on Fatigue-Crack Growth in a Metastable Beta Titanium Alloy, Ti-10V-2Fe-3Al

S.K. JHA and K.S. RAVICHANDRAN

The effect of mean stress, or the stress ratio (R), on the fatigue-crack growth (FCG) behavior of α-aged and ω-aged microstructures of the beta titanium alloy Ti-10V-2Fe-3Al was investigated. While the mean stress had a negligible effect on the FCG behavior of the α-aged microstructure, a strong effect was observed in the ω-aged microstructure. In particular, the values of the threshold stress-intensity range (ΔK_{th}) exhibited a strong dependence on R in the ω-aged microstructure, while this dependence was weak in the α-aged microstructure. These effects seem to arise primarily from fracture-surface roughness-induced crack closure. The crack closure levels for the α-aged microstructure were found to be very low compared to those for the ω-aged microstructure. Transmission electron microscopy and scanning electron microscopy studies of microstructures and fracture surfaces were performed to gain insight into the deformation characteristics and crack propagation mechanisms, respectively, in these microstructures. The microstructure-induced differences in FCG behavior are rationalized in terms of the effect of aging on slip and crack closure.

I. INTRODUCTION

TI-10V-2Fe-3Al (Ti-10-2-3), a metastable β-titanium alloy, is a widely used material for high-strength applications in the aerospace industry, owing to its relatively high strength, excellent strength/toughness combination, good fatigue strength, and enhanced processing characteristics.[1–6] A number of microstructural variations can be produced in this alloy by employing different combinations of thermomechanical processes and heat treatments.[1,2,3] Typically, the alloy is heat treated either by quenching from the $\alpha + \beta$ or the β field and is subsequently aged at a lower temperature. During aging, the β phase decomposes into a β phase enriched in β-stabilizing elements, secondary α particles (α_s), and/or ω particles, depending on the aging temperature and time.[7,8,9] By varying these parameters during aging, the strength and ductility of this alloy can be varied significantly.[1]

There are studies[1,6,8,10] indicating that fatigue crack growth (FCG) characteristics are little affected by microstructural parameters that can be varied by primary heat treatment, such as volume fraction, size, or shape of primary α in β-titanium alloys. However, there have been very few studies on the FCG behavior of Ti-10-2-3 as influenced by the secondary heat treatment, that is, the aging condition. In particular, the effect of ω-phase formation at lower aging temperatures has not been fully understood. The issue of the presence or absence of ω phase in the microstructure is significant, since it has been suggested[3,8] that ω phase formation significantly decreases the ductility of β titanium alloys. Therefore, it is considered important to systematically investigate the effect of ω phase formation on the FCG response of Ti-10-2-3, including its effect on the stress-ratio dependence of FCG behavior.

Duerig *et al.*[8] first observed a significant increase in FCG resistance at growth rates less than 5×10^{-4} mm/cycle, in the case of an ω-aged microstructure, when compared to an α-aged microstructure of comparable strength, at the stress ratio (R) of 0.1. It was suggested that planar slip induced by the ω phase led to increased mode II displacements at the crack tip, causing asperity mismatch and, thus, leading to crack closure.[11,12,13] There was no attempt, however, to show conclusively that crack closure was, indeed, responsible for the differences in the FCG behavior of ω-aged and α-aged microstructures. In the aforementioned work, at growth rates greater than 5×10^{-4} mm/cycle, the ω-aged microstructure showed higher growth rates relative to those of the α-aged microstructure. It is not obvious why a microstructure with planar deformation characteristics should show different responses above and below 5×10^{-4} mm/cycle, as indicated previously. The limited data (only one FCG test was reported) also raise concerns with regard to the dependence of FCG on R in ω-aged and ω-free microstructures in Ti-10-2-3. A study clarifying this issue is needed, since, in conventional $\alpha + \beta$ and α titanium alloys,[14–20] weak and strong effects of the stress ratio on FCG rates have been found, seemingly depending on composition and microstructures.

There are two different explanations given for the observation of a stress-ratio effect in conventional titanium alloys. First, earlier studies[14,15,16] suggested that the higher growth rates at high R levels were due to the contribution from static modes of crack extension to cyclic crack extension. Second, crack closure, due to the interference in the crack wake at low ΔK levels, has been suggested in recent studies[17,18,19] to cause lower growth rates at low R values than at high R values. However, there are also studies[20] which show that crack closure does not completely explain the stress-ratio effect on FCG rates. Further, more-recent interpretations[21] suggest an altogether different explanation for

S.K. JHA, Graduate Research Assistant, and K.S. RAVICHANDRAN, Associate Professor, are with the Department of Metallurgical Engineering, 135 South, 1460 East, Rm. 412, University of Utah, Salt Lake City, UT 84112.

Manuscript submitted May 11, 1999.

Table I. Chemical Composition of the Ti-10V-2Fe-3Al Alloy

Element	H (Max)	O (Max)	N (Max)	Fe	Al	V	Ti
Wt pct	0.01	0.03	0.03	1.93	2.95	10.15	balance

the dependence of FCG on the stress ratio. The intent of the present study is not to resolve the varied observations of stress-ratio effect and their interpretation in different classes of titanium alloys; rather, the principal objectives of this research are to investigate the effect of R on FCG in ω-aged and α-aged microstructures in Ti-10-2-3 and to identify the relevant mechanisms responsible for such an effect. Therefore, the effect of α aging *vs* ω aging on FCG was studied by maintaining a constant primary solution heat treatment and varying the nature of the secondary heat treatment. It has been found that there is only a small effect of R upon FCG in the near-threshold region, but almost none in the Paris-law regime, in the case of the α-aged microstructure. However, in the case of the ω-aged microstructure, a significant effect of the R ratio over the entire FCG regime was observed. The mechanisms responsible for these effects have been identified from fractography and crack-path observations.

II. MATERIAL AND EXPERIMENTAL PROCEDURE

A. *Material*

The Ti-10-2-3 alloy was supplied by TIMET (Henderson, NV) in the form of plates of 267 × 210 × 38 mm in size. The chemical composition of the plates is given in Table I. The β-transus temperature for the alloy was about 800 °C. The plates were made from cast ingots by the following processing routes: β forging at 850 °C, followed by air cooling, then rolling in the $\alpha + \beta$ region at 760 °C to a 25 pct reduction in thickness, followed by air cooling. The microstructures in the plates were found to be uniform through the thickness, except in the near-surface regions, to a depth of about 2 mm. These regions were removed by electrodischarge machining (EDM). Blanks cut from the plates by EDM were heat treated to obtain the desired microstructures and aged conditions. The heat-treatment schedules are given in Table II. Since the strength of the Ti-10-2-3 alloy is largely influenced by aging, the aging periods were appropriately chosen to obtain similar strength levels at different aging temperatures. This was done to minimize the variation in FCG behavior due to differences in the strength level. Since the objective was to have comparable strength levels, the ω aging period was restricted to 6 hours. This may not correspond to complete transformation of β at this temperature. However, microhardness studies indicated that the change in Vickers hardness after 6 and 32 hours of aging treatment was less than 17 pct, suggesting that most of the transformation had occurred within 6 hours. Therefore, the microstructure can be considered to be almost in equilibrium. Compact-tension (CT) specimens of 63.5 × 61 × 8 mm in size, oriented in the longitudinal-transverse direction, were machined from the heat-treated blanks. The specimen surfaces were metallographically polished down to 1 μm alumina to enable the observation of crack growth.

B. *Experiments*

The FCG tests were conducted in an MTS 810 servohydraulic fatigue test system equipped with a TESTSTAR II digital controller, a personal computer, and the associated test-control software. Tests were done following the ASTM E647-93 FCG test standard.[22] The samples were precracked at ΔK levels of about 10 to 15 MPa$\sqrt{\text{m}}$. Following precracking, a decreasing ΔK test and, subsequently, an increasing ΔK test were conducted on a given sample. The ΔK gradients[22] of -0.08 and 0.2 were employed in the decreasing and increasing ΔK tests, respectively. Tests were performed at three stress ratios ($R = 0.1$, 0.5, and 0.8) at the frequency of 35 Hz, at room temperature in a laboratory air environment. Crack lengths were continuously monitored during testing using a crack-opening displacement (COD) gage* mounted at the mouth of the notch. The COD gage also enabled continuous recording of the load *vs* displacement traces, from which the closure loads were determined. The point of initial deviation from the linear-elastic part of the unloading curves was taken to be the closure load. These closure loads were used to determine ΔK_{eff} and K_{cl} values. The FCG tests were repeated at each R ratio to ensure reproducibility of the FCG data. In the case of the ω-aged microstructure, in addition to tests on regular CT samples, tests were also conducted using side-grooved CT samples. This was because, in regular CT samples, crack-plane deviations of about 10 deg occurred sometimes when cracks grew out of the notch. The K calculations for side-grooved specimens

*Model No. MTS 632.02F-20.

Table II. Heat Treatments, Microstructural Descriptions, and Tensile Properties for the Microstructures Investigated

Designation	Heat Treatment	Microstructure	0.2 Pct Yield Strength (MPa)	UTS (MPa)	Pct Elongation
α-aged	solution treatment at 700 °C for 2 h followed by water quenching; aging treatment at 525 °C for 8 h followed by water quenching	45 pct $\alpha_p + \alpha_s$ particles in β-matrix	987	1065	13
ω-aged	solution treatment at 700 °C for 2 h followed by water quenching; aging treatment at 260 °C for 6 h followed by water quenching	45 pct $\alpha_p + \omega$ particles in β-matrix	1028	1047	9

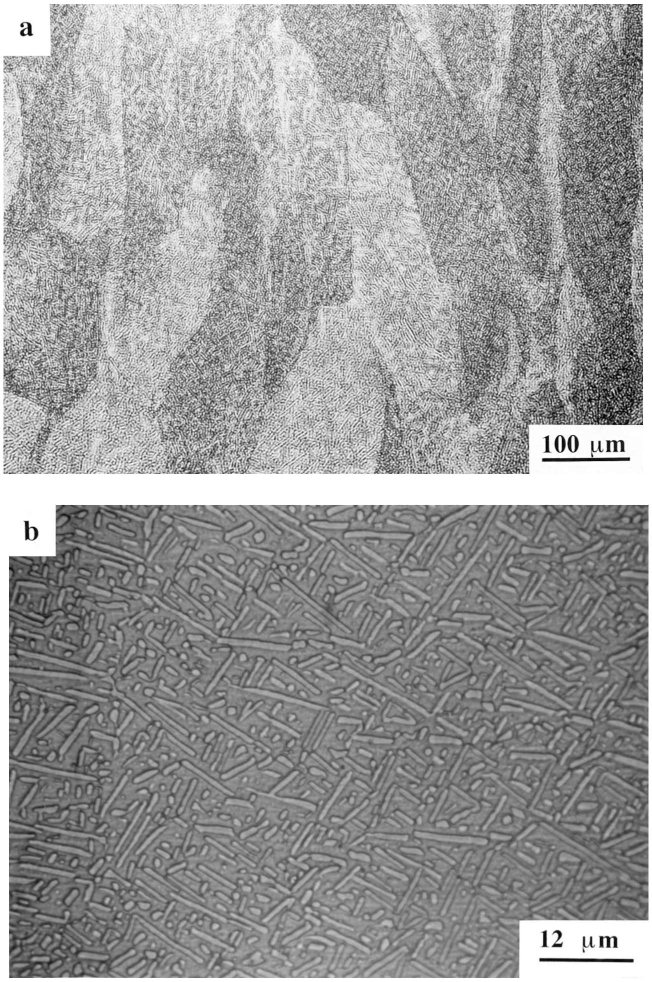

Fig. 1—Optical micrographs of the α-aged microstructure (*a*) showing prior-β grains and (*b*) showing distribution of α_p particles.

were done following ASTM E813-89 standards. Since there was no difference between the FCG behavior as determined by CT and side-grooved CT specimens, it was concluded that neither the side grooves nor the small out-of-plane crack extensions affected the FCG behavior of the ω-aged microstructure. The fracture surfaces, as well as crack-path profiles of FCG samples obtained by sectioning the fracture surface along the plane parallel to the specimen broad surface, were observed in a Cambridge S240 scanning electron microscope at an accelerating voltage of 20 kV. Thin-foil specimens, for observations of microstructure in a transmission electron microscope (TEM), were prepared by dimpling followed by ion milling. The foils were observed in a JEOL** JEM-2000 FX II TEM, at an accelerating voltage of 200 kV.

**JEOL is a trademark of Japan Electron Optics Ltd., Tokyo.

III. RESULTS AND DISCUSSION

A. *Microstructural and Tensile Properties*

Optical micrographs of the α-aged microstructure are shown in Figures 1(a) and (b). Figure 1(a) illustrates the structure of the β grains, which are elongated in the rolling direction. Figure 1(b) shows the morphology and the distribution of primary α (α_p) particles. Since the primary α heat treatment was the same, both the α-aged and the ω-aged microstructures appeared similar in optical micrographs. The volume fraction and the average interparticle spacing of α_p particles were estimated to be 0.45 and 1.8 μm, respectively, using point-counting and linear-intercept methods.[23] The microstructures, however, differed in terms of the constituents in the transformed β matrix. In Figure 2, TEM micrographs of the transformed β microstructure in the α-aged condition are presented. The bright-field micrograph and the $(110)_\beta$ diffraction pattern of this region are presented in Figures 2(a) and (b), respectively. The schematic of the diffraction pattern, presented in Figure 2(c), indicates that the (0001) pattern of secondary α (α_s) particles in the transformed β matrix is superimposed on the β-phase pattern. This is consistent with the established orientation relationship[7,24] between the α and β phases in titanium alloys, *viz.*, $(0001)_\alpha//\{110\}_\beta$ and $\langle 11\bar{2}0\rangle_\alpha//\langle 111\rangle_\beta$. Campagnac and Vassel[7] observed a slight arcing of the α_s diffraction spots in the diffraction pattern of an α-aged matrix. They concluded that this occurred due to superposition of two $(0001)_{\alpha_s}$ patterns. However, arcing was not very evident in the present study (Figure 2(b)). Dark-field imaging using the $(1\bar{1}00)_{\alpha_s}$ spot revealed the presence of relatively coarse α_s particles in the matrix (Figure 2(d)). In Figure 3, TEM micrographs of the ω-aged microstructure are presented, showing the distribution of ω phase in the ω-aged microstructure. The bright-field micrograph and the $(110)_\beta$ pattern of this region are presented in Figures 3(a) and (b), respectively. It is clear from Figure 3(b) that the $(11\bar{2}0)_\omega$ pattern is superimposed on the β-phase pattern (Figure 3(c)). This also is consistent with the established orientation relationship[7,24] between the ω and β phases in titanium alloys, *viz.*, $(0001)_\omega//\{111\}_\beta$ and $\langle 11\bar{2}0\rangle_\omega//\langle 110\rangle_\beta$. The dark-field image formed using the $(10\bar{1}0)_\omega$ spot revealed the distribution of ω phase in the matrix (Figure 3(d)).

B. *Effect of Stress Ratio on FCG*

Figures 4(a) and (b) show the FCG data for the stress ratios of $R = 0.1$, 0.5, and 0.8, in the form of da/dN *vs* ΔK plots, for the α-aged and ω-aged microstructures, respectively. From repeated tests, the FCG behavior was found to be very reproducible for both microstructures. For the α-aged microstructure, a smaller effect of R was observed in the near-threshold region, and very little R effect was present in stage II (Paris-law regime) of FCG. Such a pattern is commonly seen in high-strength materials, including 2.25Cr-1Mo steel[25] and some Al alloys.[26] Additionally, these data are consistent with the reported FCG data on the Ti-10-2-3 alloy.[27] In contrast, a significant R effect was observed, both in the threshold regime and in the Paris-law regime of FCG, for the ω-aged microstructure. Figure 5 shows the FCG data in terms of da/dN *vs* ΔK_{eff} for the two microstructures. It can be seen that the stress-ratio effect vanishes when the FCG data are plotted in terms of ΔK_{eff}, although, for the ω-aged microstructure at R equal to 0.8, the crack growth rates are slightly higher at da/dN levels greater than 10^{-4} mm/cycle. This suggests that the observed stress-ratio effect in most of the FCG region in the two microstructures is due to crack closure. It then follows that the ω-aged microstructure exhibited a

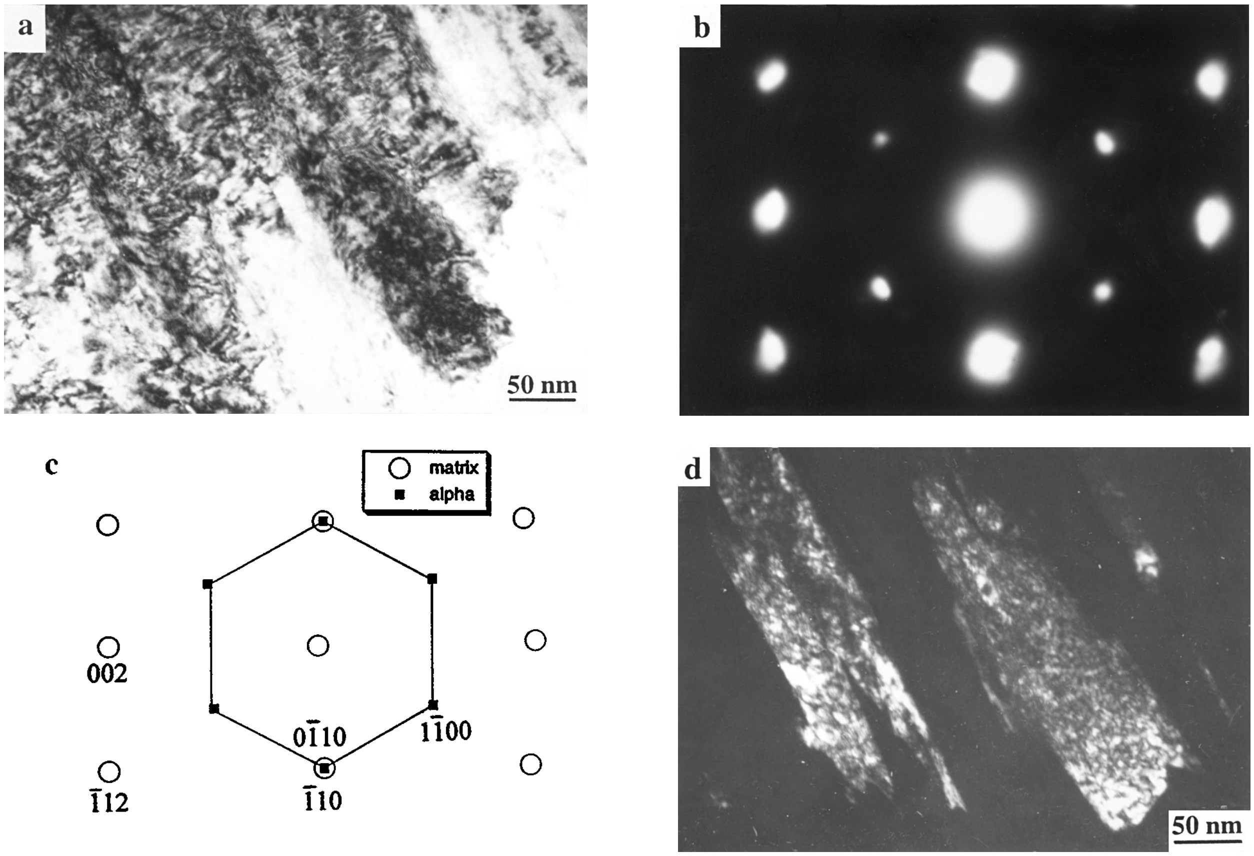

Fig. 2—TEM micrographs of the α-aged microstructure: (*a*) bright-field image, (*b*) $[110]_\beta$ zone diffraction pattern, (*c*) indexed diffraction pattern, and (*d*) dark-field image using the $(1\bar{1}00)_{\alpha s}$ spot.

greater degree of crack closure compared to the α-aged microstructure. It also follows that there is very little difference between the FCG behavior of the α-aged and ω-aged microstructures once closure is accounted for.

C. *Effect of Stress Ratio on* ΔK_{th}

The effect of stress ratio on the threshold condition for FCG in the two microstructures is summarized in Figure 6 in the form of ΔK values at threshold (ΔK_{th}) and ΔK_{eff} values at threshold ($\Delta K_{\text{eff},th}$), plotted as a function of R. It is clear from Figure 6 that there is a greater effect of stress ratio on ΔK_{th} in the ω-aged microstructure than in the α-aged microstructure. The effect of the stress ratio vanishes when $\Delta K_{\text{eff},th}$ is considered instead of ΔK_{th}. In order to compare the closure levels at $R = 0.1$ in the two microstructures, the closure stress-intensity levels (K_{cl}) are plotted as a function of $K_{\min}$ in Figure 7. It is clear that considerably higher K_{cl} values were observed in the ω-aged microstructure than in the α-aged microstructure. While no crack closure was observed for ΔK levels greater than about 19 MPa$\sqrt{\text{m}}$ ($K_{\min}$ greater than about 2.1 MPa$\sqrt{\text{m}}$) in the α-aged microstructure at $R = 0.1$, substantial closure levels were observed even at higher ΔK values in the ω-aged microstructure. At $R = 0.5$, while no crack closure was observed in the α-aged microstructure, considerable closure was observed in the ω-aged microstructure (Figure 7). At $R = 0.8$, the *da*/*dN vs* ΔK_{eff} data were the same as the *da*/*dN vs* ΔK curve, for both microstructures, because of the absence of crack closure at $R = 0.8$.

D. *Effect of Microstructure on FCG Behavior*

A comparison of FCG behavior at $R = 0.1$ for the two microstructures is made in Figure 8. In Figure 8(a), the FCG data are presented in terms of *da*/*dN vs* ΔK. The relatively lower crack growth rates in the ω-aged microstructure (Figure 8(a)) are due to higher levels of crack closure in this microstructure, as discussed in the previous section. In Figure 8(b), comparison is made between the two microstructures in terms of *da*/*dN vs* ΔK_{eff} data. Once closure is accounted for, the data for the two microstructures come together, except for some difference in the threshold region of FCG (Figure 8(b)). Figure 9 shows the *da*/*dN vs* ΔK data at $R = 0.8$ for the two microstructures. As one would expect, in the absence of fatigue-crack closure, the two curves agree well, although there is a small difference in the threshold region of FCG. This difference must be due to microstructural effects. It has been suggested[28] that crack deflection at the microstructural level leads to the realization of a mode I ΔK that is smaller than the applied ΔK. The FCG rate differences observed only in the near-threshold region of FCG are also consistent with the fact that crack deflections from the mode I growth plane become significant only in the near-threshold regime, where increased mode II displacements become operative at the crack tip, due to localization

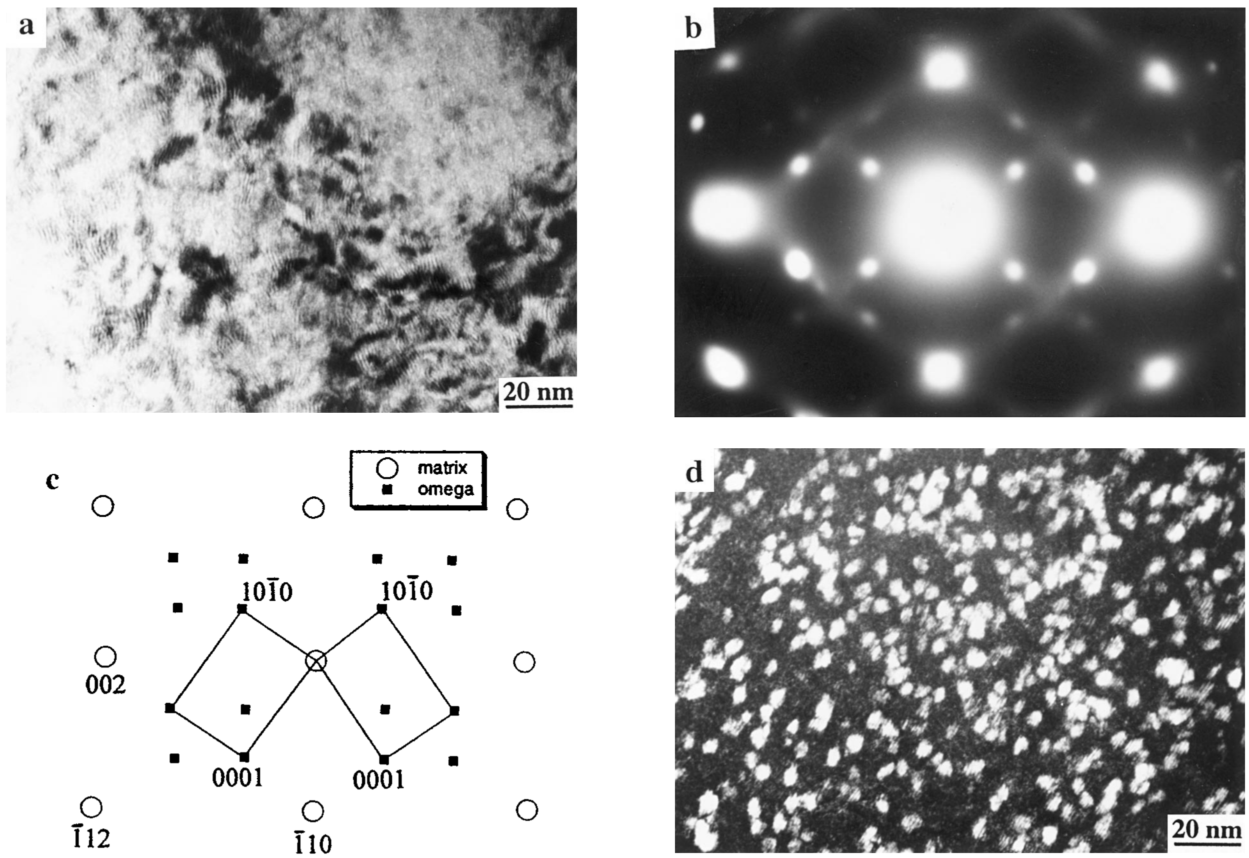

Fig. 3—TEM micrographs of the ω-aged microstructure: (*a*) bright-field image, (*b*) $[110]_\beta$ zone diffraction pattern, (*c*) indexed diffraction pattern, and (*d*) dark-field image using the $(10\bar{1}0)_\omega$ spot.

of crack-tip deformation along slip bands. In any case, this effect could not be attributed to the macroscopic crack-plane deviations observed in the FCG tests of the ω-aged microstructure. This is because of the fact that the FCG test data from regular CT and side-grooved CT specimens agreed well with each other.

E. *Fatigue Fracture Mechanisms in the Near-Threshold Region*

The fracture morphologies observed in the near-threshold region are shown in Figures 10 and 11 for the α-aged and ω-aged microstructures, respectively. At a relatively low magnification, a flat, transgranular fracture surface was observed in the α-aged microstructure (Figure 10(a)) tested at $R = 0.1$. At a higher magnification, well-defined traces of α_p particles were seen (Figure 10(b)). In addition, a fracture morphology consisting of microscopically small features, the size of which roughly corresponded to the average α_p interparticle distance (1.86 μm), was seen (Figure 10(c)). In contrast, in the ω-aged microstructure, a rough fracture-surface topography was evident even at a low magnification level (Figure 11(a)). The sizes of these roughness features nearly corresponded to the average prior-β grain size (Figure 1(a)). At a higher magnification, however, traces of α_p particles were seen in these regions. These traces were not very well defined, but appeared to be irregular and discontinuous and seem to consist of secondary cracks (Figure 11(b)).

It is now well known[11–13,29,30] that, in the near-threshold FCG region, crack propagation is accomplished by dislocation movement by mode II shear at the crack tip. Generally, a single slip system is suggested to be active,[11,12,30] promoting a zigzagged crack path in polycrystalline materials.[11,12,30] In this study, the relatively high fracture-surface roughness observed in the ω-aged microstructure suggests that the dislocation pileup lengths were on the order of the prior-β grain size, with the crack deflecting at the prior-β grain boundaries, during crack growth. To verify this in the ω-aged microstructure, profiles of the crack path were examined in detail in the three regimes of ΔK, *viz.*, the decreasing ΔK regime, the near-threshold regime, and the increasing ΔK regime. Figures 12(a) through (d) illustrate the crack-path profiles in each of these regimes and the corresponding normalized crack closure levels ($K_{cl}/K_{\max}$) plotted as a function of crack length. The crack length and the ΔK levels corresponding to the crack-tip positions at the centers of the figures are also indicated. While the crack-path profiles in the decreasing ΔK (Figure 12(a)) and in the increasing ΔK regimes (Figure 12(c)) appeared flat, the profile in the threshold regime was found to be rough (Figure 12(b)). Evidence of crack deflections at grain boundaries is seen, as indicated by the points marked as A in Figure 12(b). At the points marked as B however, cracks deflected within a grain. This kind of deflection seemed to occur in a relatively larger grain. In Figure 12(d), the closure level increased during the decreasing ΔK test, reached a maximum at the threshold region ($da/dN \sim 10^{-7}$ mm/cycle), and then decreased during the increasing ΔK test. In contrast, the

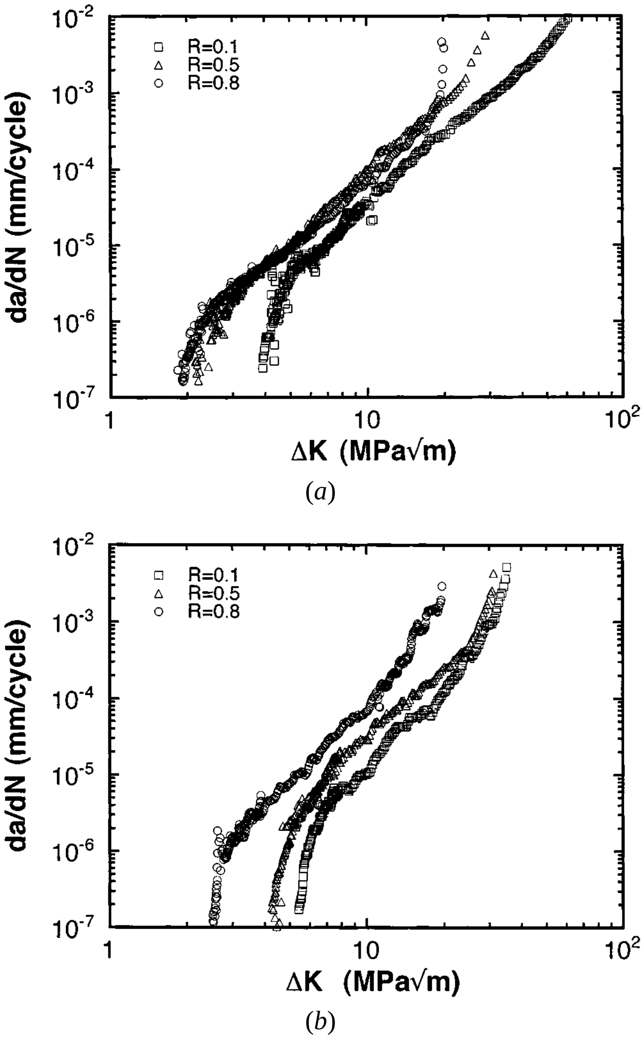

Fig. 4—The effect of stress ratio on the FCG behavior of (*a*) α-aged microstructure and (*b*) ω-aged microstructure.

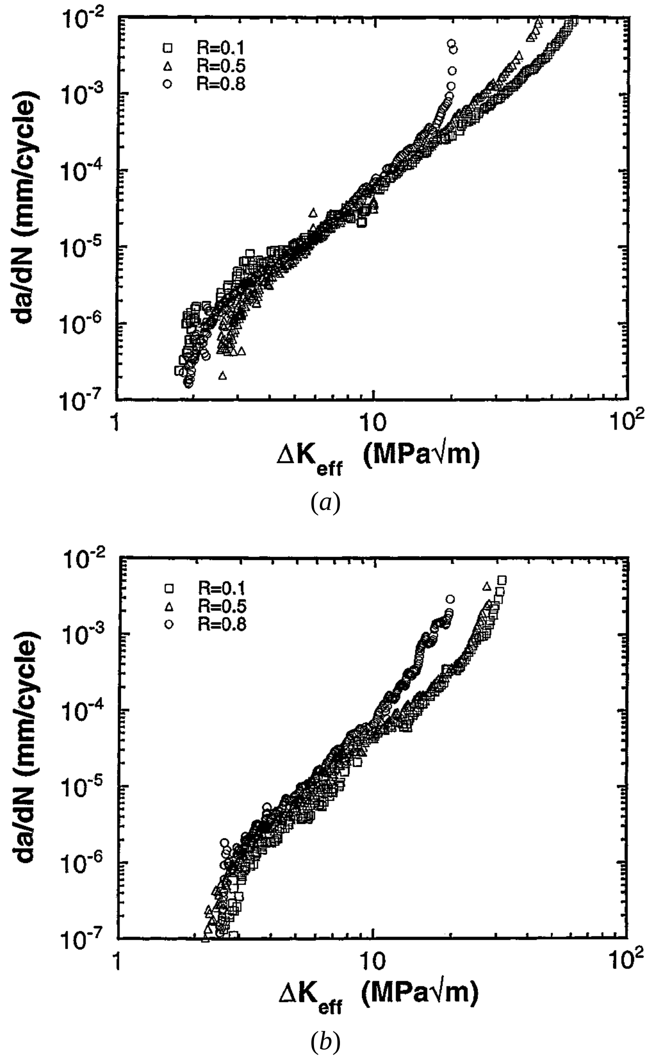

Fig. 5—The FCG data plotted in terms of ΔK_{eff} for (*a*) α-aged microstructure and (*b*) ω-aged microstructure.

crack-path profile in the α-aged microstructure (not presented here) was flat throughout the entire ΔK regime. This is expected, based on observations made on the fracture surfaces of the α-aged microstructure (Figure 10(a)). A flat crack-path profile over the entire range of applied ΔK and the observation of well-defined traces of α_p (Figure 10(b)), as well as the presence of features corresponding to the α_p interparticle spacing (Figure 10(c)), suggest that crack deflections on the order of α_p interparticle spacing occurred during crack growth in the α-aged microstructure.

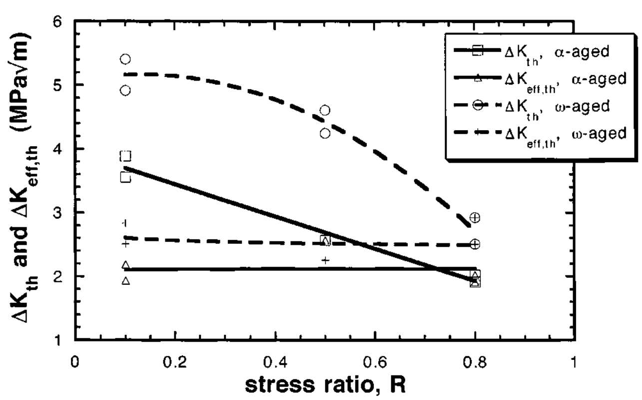

Fig. 6—The effect of stress ratio on ΔK_{th} and $\Delta K_{\text{eff},th}$ for the α-aged and ω-aged microstructures.

F. *Effect of Microstructure on Crack Closure*

It is important to rationalize the fracture-surface roughness levels on the basis of crack-tip deformation, controlled by the interactions between dislocations and microstructural features. As has been documented in many studies,[31,32,33] small, coherent and shearable ω particles tend to produce planar slip during deformation at relatively low temperatures. It appears that the increased fracture-surface roughness in the ω-aged microstructure is caused by planar slip. It is evident from Figures 2(d) and 3(d) that the ω particles in the ω-aged microstructure are relatively smaller than the α_s particles in the α-aged microstructure. Furthermore, the ω phase has an ordered hcp crystal structure.[34,35,36] These ordered ω particles would be expected to dominate the deformation behavior due to their high density in the matrix

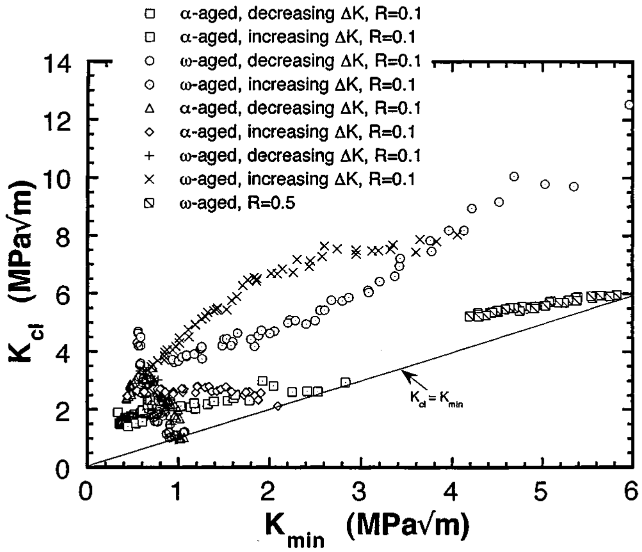

Fig. 7—The crack closure data, K_{cl}, plotted as a function of $K_{\min}$, for the α-aged and ω-aged microstructures.

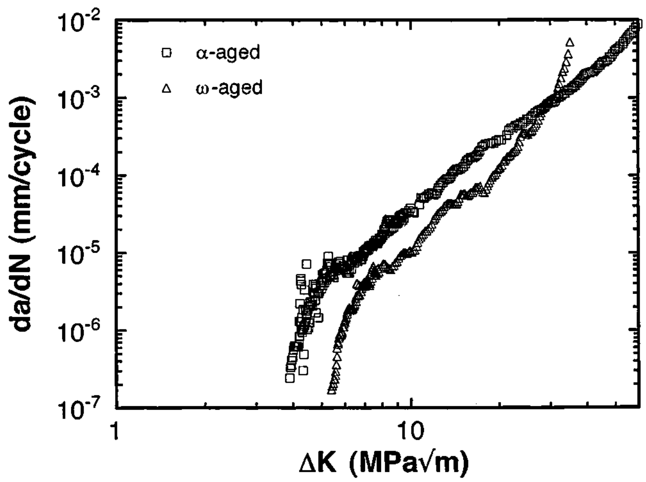

(*a*)

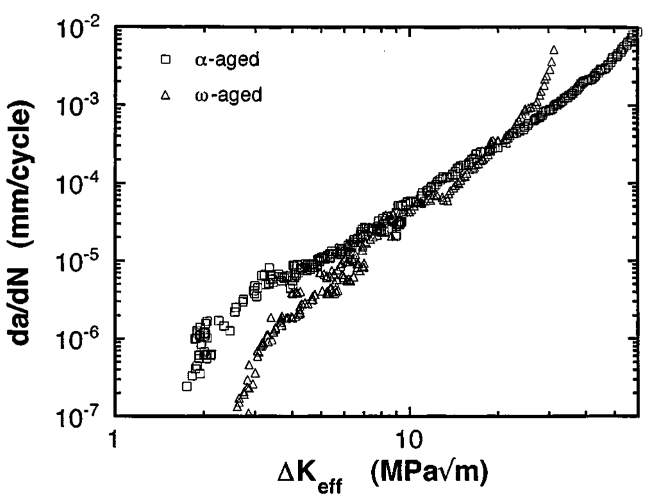

(*b*)

Fig. 8—A comparison of FCG behavior of α-aged and ω-aged microstructures at $R = 0.1$: (*a*) in terms of da/dN *vs* ΔK and (*b*) in terms of da/dN *vs* ΔK_{eff}

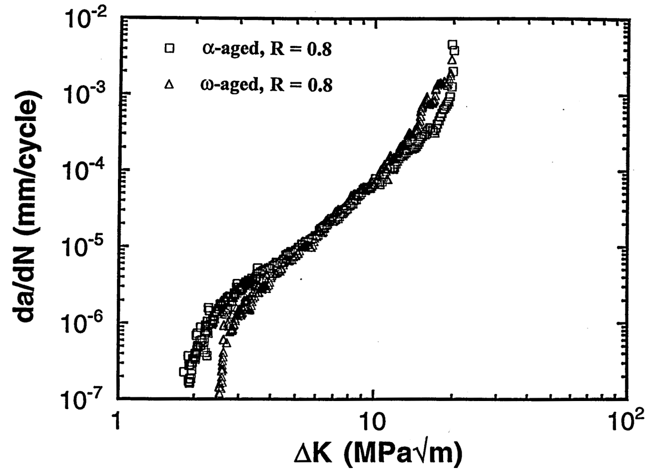

Fig. 9—A comparison of FCG behavior of α-aged and ω-aged microstructures at $R = 0.8$.

(Figure 3(d)). This is expected to cause an enhanced localization of dislocation motion in the ω-aged matrix when compared to the α-aged matrix. It seems that such localized deformation causes shearing of α_p particles in the ω-aged microstructure (Figure 11(a)). In the α-aged microstructure, however, only homogenous slip is expected to occur, thus leading to a more homogenous distribution of deformation in the matrix. This seems to result in crack growth by cleavage either through the α_p particles or along the α_p-matrix interfaces (Figure 10(b)). On the basis of this reasoning, the mechanisms of crack propagation are illustrated schematically for the α-aged and ω-aged microstructures in Figures 13(a) and (c), respectively. The crack-path profiles in the near-threshold region of the α-aged and the ω-aged microstructures are presented in Figures 13(b) and (d), respectively. The presence of large-sized asperities in the crack path of the ω-aged microstructure (Figure 13(b)) supports the suggested FCG mechanism. The crack-path profile appears to be more or less flat for the α-aged microstructure (Figure 13(d)), even at a magnification level higher than that of Figure 13(b), indicating the very small sizes of fracture-surface asperities in the α-aged case, relative to the ω-aged microstructure.

On the basis of the fracture mechanisms discussed previously, it is possible to conclude that crack closure was primarily caused by fracture-surface roughness. Due to shear across many α_p platelets, larger facets were formed in the ω-aged microstructure and the fracture-surface roughness was controlled by the prior-β grain size. On the other hand, in the α-aged microstructure, the α_p interparticle spacing, which was much smaller than the β grain size, controlled the fracture-surface roughness. This difference appears to cause the different closure responses in the two cases at $R = 0.1$. It is also important to discuss the high closure levels observed in the ω-aged microstructure in the Paris-law regime ($10^{-5} \leq da/dN \leq da/dN < 10^{-3}$ mm/cycle) of crack growth. Figure 14 shows a comparison of closure levels in the two microstructures over the entire range of applied ΔK levels. The closure levels are plotted in terms of $(K_{cl} - K_{\min})/K_{\min}$, in order to show by what factor K_{cl} exceeded $K_{\min}$ during FCG. It is interesting to note that, initially, both microstructures exhibited comparable closure levels at the begining of the decreasing ΔK

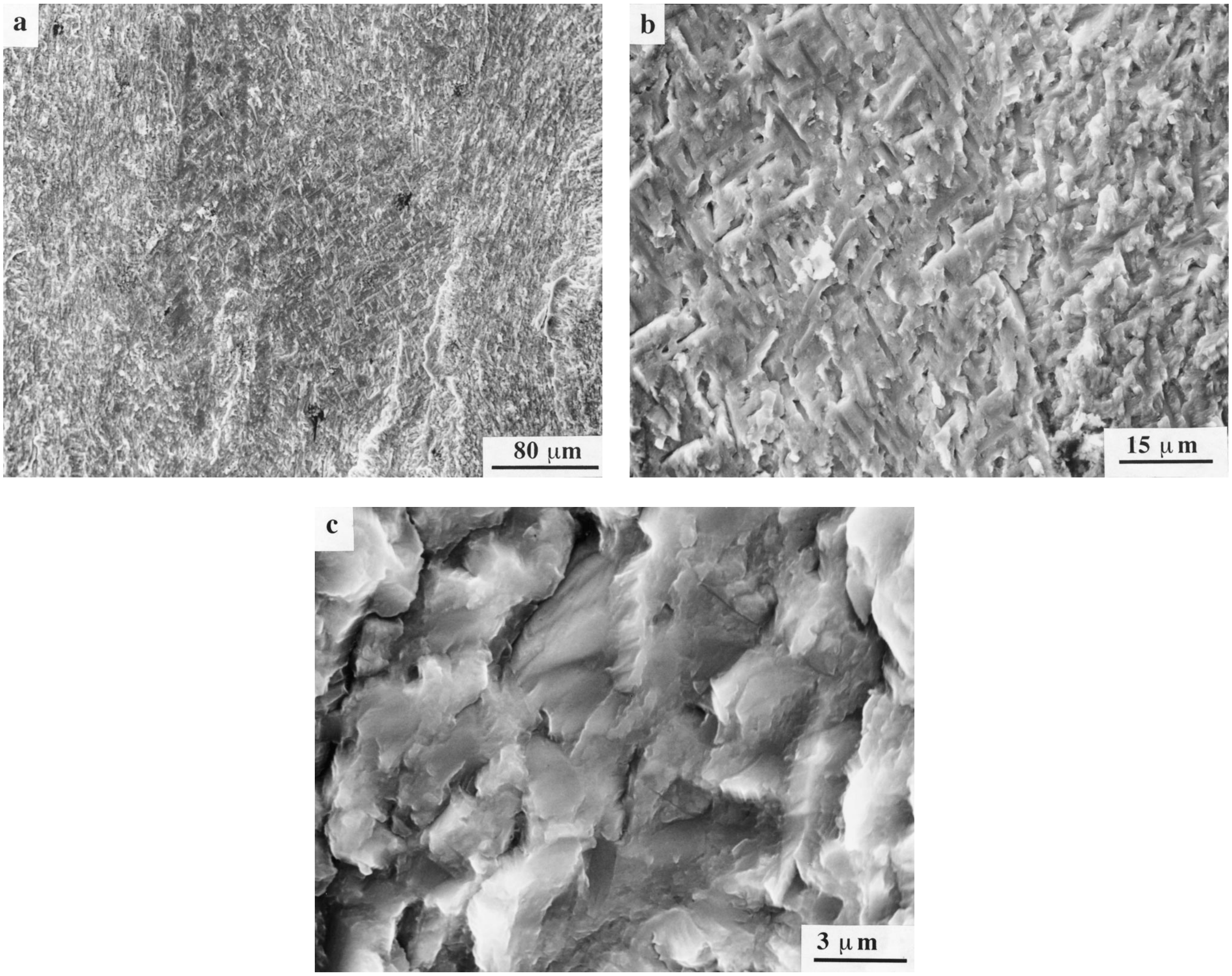

Fig. 10—Fracture topography in the α-aged microstructure in the near-threshold region: (*a*) at a low magnification, (*b*) showing well-defined traces of α_p particles, and (*c*) at a high magnification revealing features having sizes of the order of α_p interparticle distances.

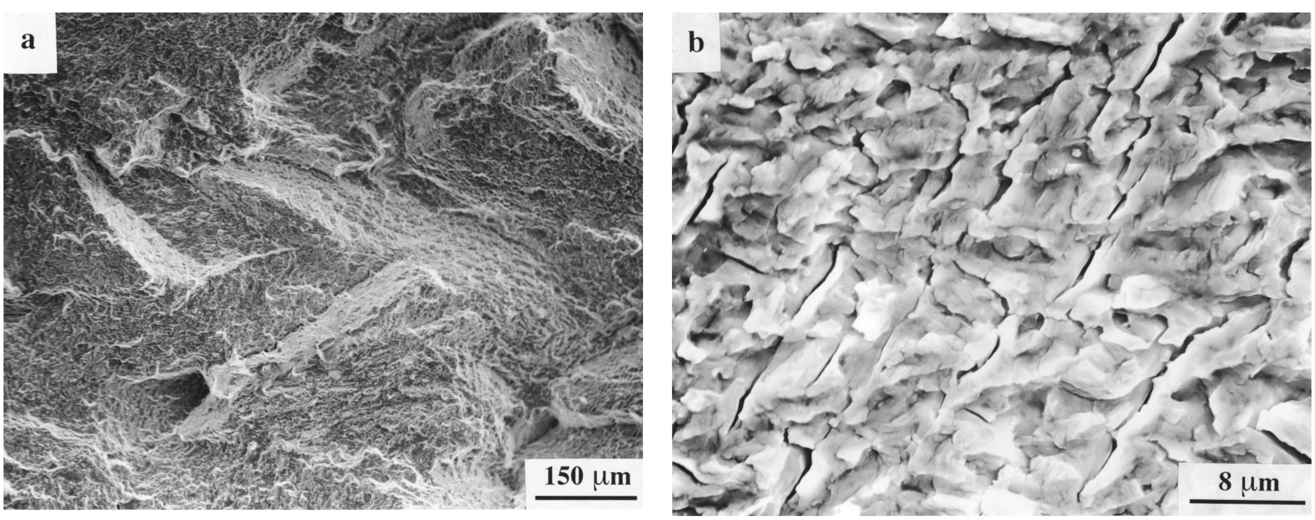

Fig. 11—Fracture topography in the ω-aged microstructure in the near-threshold region: (*a*) at a low magnification revealing the roughness features and (*b*) revealing the traces of α_p particles.

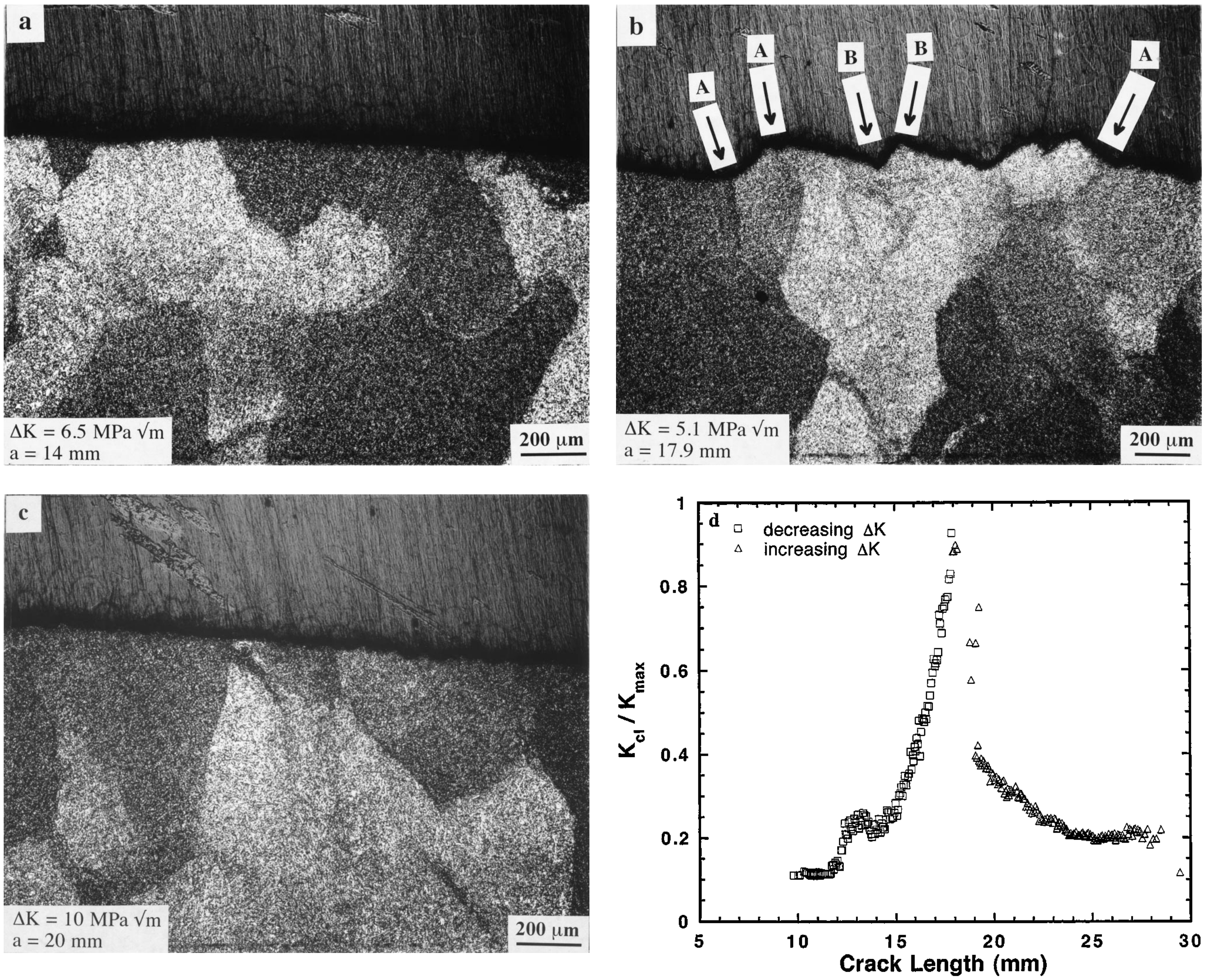

Fig. 12—Crack path profiles and normalized closure levels as a function of crack length in the ω-aged microstructure: (*a*) decreasing ΔK test, $\Delta K = 6.5$ MPa$\sqrt{m}$, $a = 14$ mm; (*b*) threshold region, $\Delta K = 5.1$ MPa$\sqrt{m}$, $a = 17.9$ mm; (*c*) increasing ΔK test, $\Delta K = 10$ MPa$\sqrt{m}$, $a = 20$ mm; and (*d*) K_{cl}/K_{max} plotted as a function of crack length in the ω-aged microstructure at $R = 0.1$.

tests. However, due to the high fracture-surface roughness that formed in the near-threshold region, a significantly higher closure level was seen in the ω-aged microstructure. The ($K_{cl} - K_{min}$) values are about 5 and 8 times K_{min} for the α-aged and the ω-aged microstructures, respectively. However, during the increasing ΔK part after ΔK_{th}, the closure levels are no longer similar in the two microstructures. The closure levels are significantly higher in the ω-aged microstructure than in the α-aged microstructure. This is understandable, since the fracture-surface roughness that was formed near the threshold can continue to interfere with the opening and closing of the crack, even after the crack had propagated significantly under increasing ΔK conditions. The presence of closure ($K_{cl} > K_{min}$), even at $R = 0.5$ in the ω-aged microstructure, can be rationalized. The average height of asperities in the near-threshold region of the ω-aged microstructure was found to be about 125 μm (Figure 13), whereas the maximum crack-mouth opening displacement (CMOD) in the near-threshold region at $R = 0.5$ was 70 μm. The maximum crack opening level is clearly smaller than the average height of the asperities. Therefore, partial closure of cracks, even at $R = 0.5$, is expected. On the other hand, in the α-aged microstructure, the height of the fracture-surface asperities seems to correspond to the average α_p interparticle distance, *i.e.*, 1.8 μm. This is much smaller than the minimum CMOD encountered in the near-threshold region, which was 28 μm. Therefore, the fracture-surface roughness levels provide a rationale for the different closure levels observed at $R = 0.1$ and 0.5, in the two microstructures.

G. *Fatigue Fracture Mechanisms in the Paris-Law Region*

The fracture modes observed in the Paris-law regime ($10^{-5} \leq da/dN \leq 10^{-3}$ mm/cycle) of crack growth at $R = 0.1$ are shown in Figures 15 and 16 for the α-aged and ω-aged microstructures, respectively. In the α-aged microstructure, considerable secondary cracking perpendicular to the crack-propagation direction was observed (Figure 15(a)). The secondary cracks did not correlate to the dimensions of α_p particles. As suggested by Yoder *et al.*,[37] the secondary cracks might have occurred along slip bands. However, it

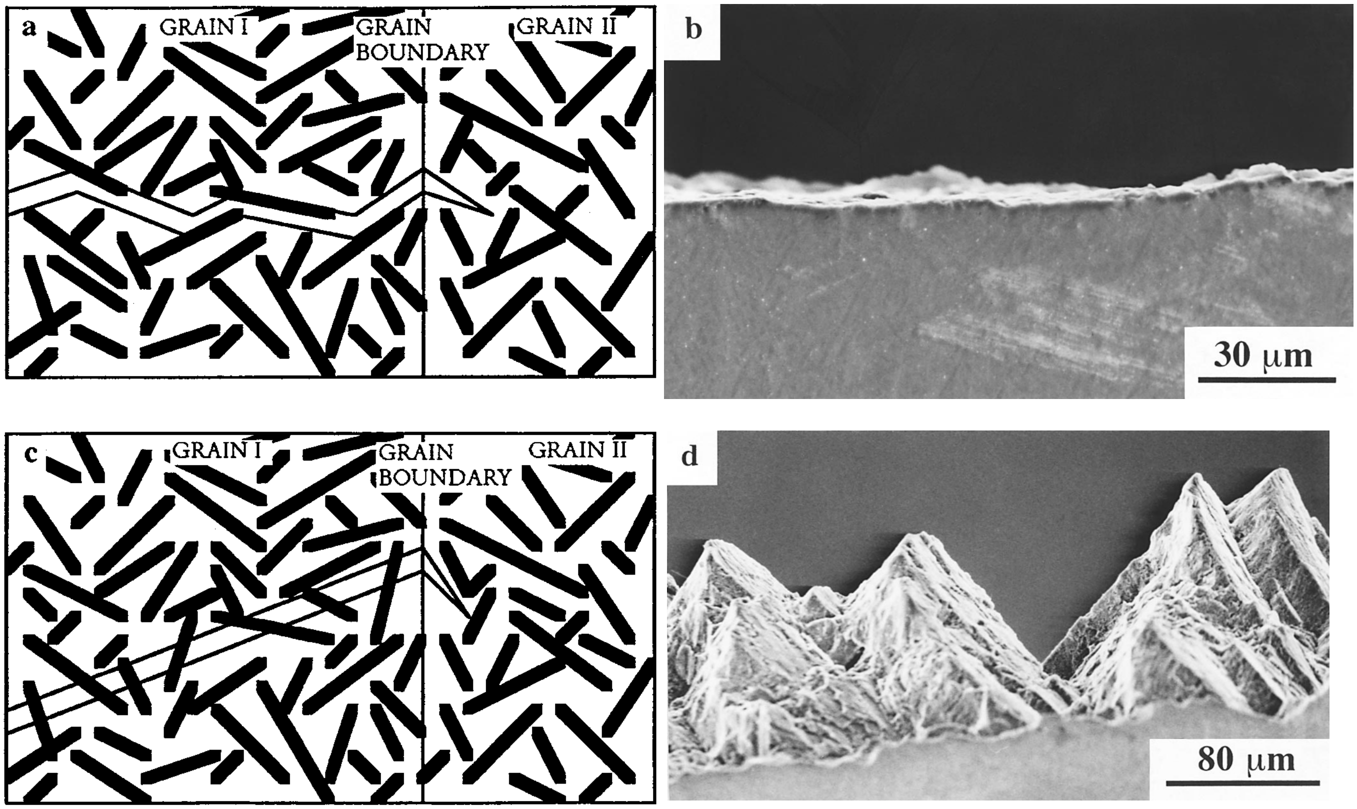

Fig. 13—Aschematic of the fatigue crack propagation mechanism in (*a*) α-aged and (*c*) ω-aged microstructures. The crack path profiles in the near-threshold region; these microstructures are shown in (*b*) and (*d*), respectively.

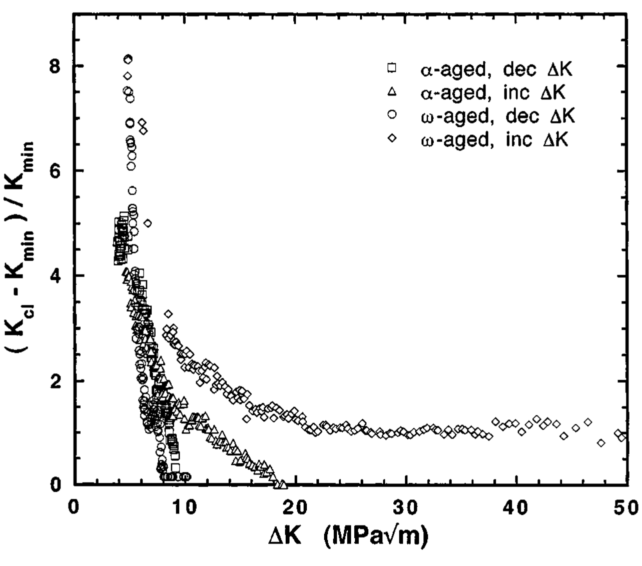

Fig. 14—The relative crack closure level $((K_{cl} - K_{\min})/K_{\min})$ plotted as a function of ΔK, for the α-aged and ω-aged microstructures.

is not possible to conclude whether secondary cracks occurred at the α_p/β interfaces or along the slip bands. Besides secondary cracks, fatigue striations were also observed at high ΔK levels (Figure 15(b)). In the ω-aged case, on the other hand, there was almost no secondary cracking, with the exception of a few cracks at random locations, in the Paris-law regime (Figure 16(a)). At a higher magnification, (Figure 16(b)), the fracture surface appeared to consist of coarse slip steps accompanied by striation-like features. It was not possible to resolve the striations.

The monotonic crack-tip plastic-zone sizes ($r_m = (1/3\pi)(K_{\max}/\sigma_{ys})^2$, where σ_{ys} is the yield stress) in the Paris-law ΔK regime ($10^{-5} \leq da/dN \leq 10^{-3}$ mm/cycle) were estimated to be greater than at least 16 μm in both microstructures. Therefore, the crack-tip plastic zone was larger than the average α_p interparticle distance. It is possible that this is the reason why α_p traces were absent in the fracture surfaces in this regime in both the microstructures. Even though the fracture-surface roughness in the Paris-law regime in the ω-aged microstructure was low, the fracture-surface roughness introduced in the near-threshold region influenced the crack closure during crack growth in this regime during increasing ΔK tests. Therefore, a significant effect of R on the crack growth rate resulted in high ΔK levels in the ω-aged microstructure. Such an effect was absent in the α-aged microstructure due to the very small roughness features in near-threshold region.

IV. CONCLUSIONS

1. A strong effect of stress ratio on fatigue-crack growth behavior, in particular, on the crack growth rates, was observed in the ω-aged condition of a Ti-10V-2Fe-3Al alloy when compared to the α-aged condition of the alloy.
2. The stress-ratio effect could, to a large extent, be explained on the basis of roughness-induced crack closure. When there was a high level of closure (ω-aged microstructure), the crack growth rates were strongly

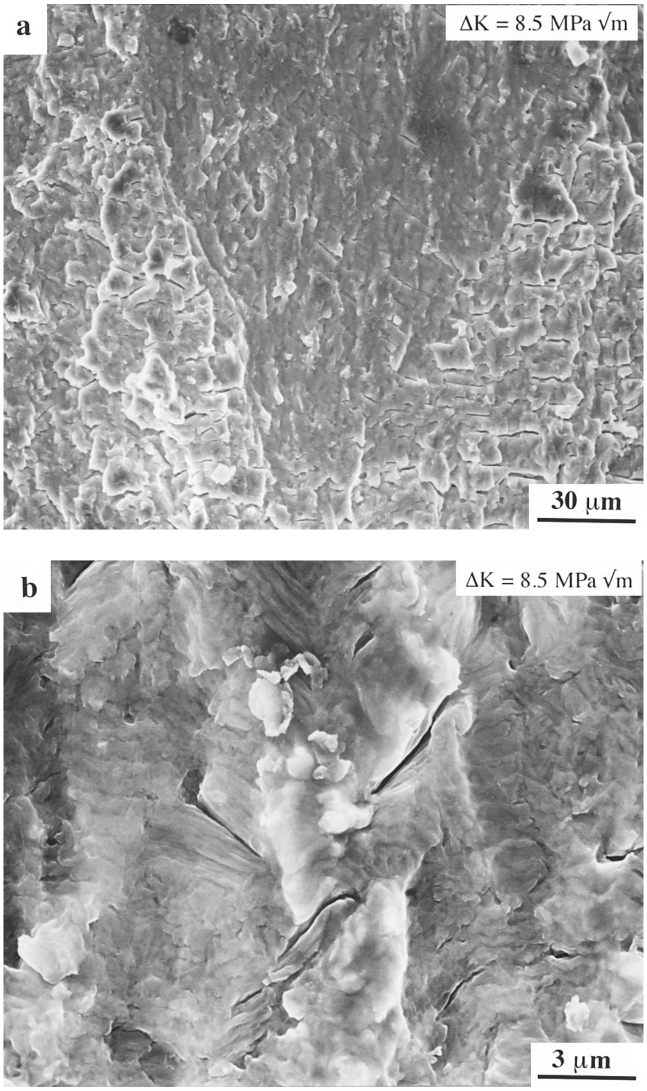

Fig. 15—Fracture topography in Paris-law regime as observed in the α-aged microstructure at (*a*) a low magnification and (*b*) a high magnification.

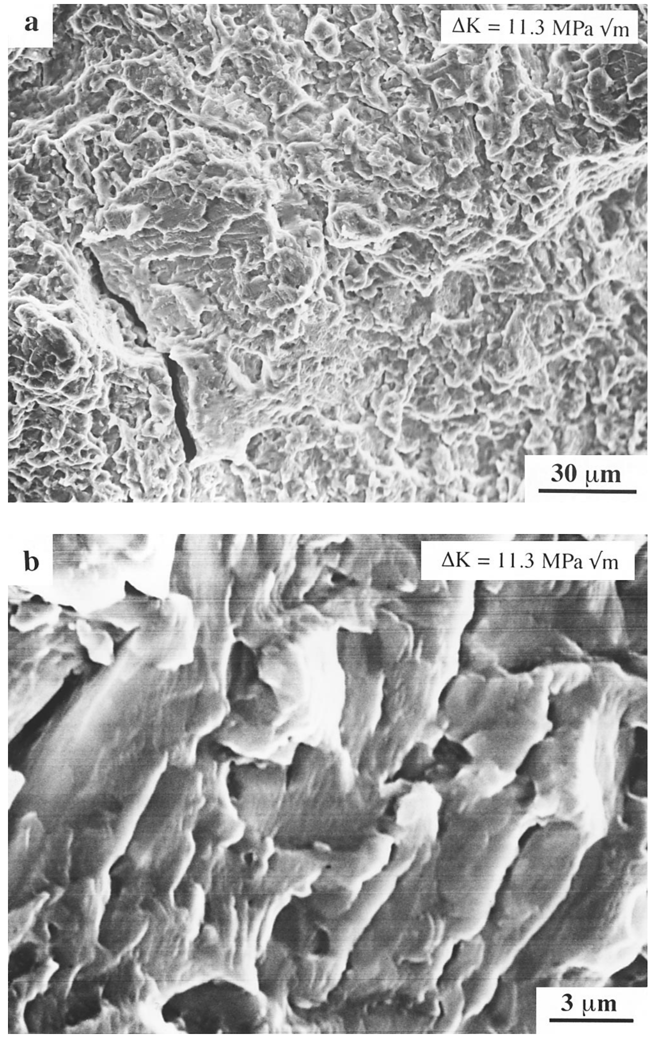

Fig. 16—Fracture topography in the Paris-law regime as observed in the ω-aged microstructure at (*a*) a low magnification and (*b*) a high magnification.

dependent on the stress ratio. When there was low closure (α-aged microstructure), the crack growth rates were almost independent of the stress ratio.

3. The fracture-surface roughness features near the threshold in the ω-aged microstructure were found to correspond to the prior-β grain size. In the α-aged microstructure, however, fracture-surface roughness features corresponded to the α_p interparticle spacing. The prior-β grain size and the α_p interparticle spacing were the microstructural units controlling crack growth rates in the ω-aged and the α-aged microstructures, respectively. This suggestion is consistent with the microstructural characteristics, deformation modes, and the crack-path profiles observed during fatigue-crack growth.

ACKNOWLEDGMENTS

The authors sincerely acknowledge the support of the Structural Materials Program, Air Force Office of Scientific Research (AFOSR, Washington, DC) through Grant No. F49620-96-1-0102. The authors appreciate the interest and encouragement of Drs. C.H. Ward and S. Wu of this organization. The provision of material by TIMET is gratefully acknowledged. In particular, the authors thank C. Clay and P. Allen, TIMET, in this regard.

REFERENCES

1. R.R. Boyer and G.W. Kuhlman: *Metall. Trans. A*, 1987, vol. 18A, pp. 2095-2103.
2. G. Terlinde, H. J. Rathjen, and K.H. Schwalbe: *Metall. Trans. A*, 1986, vol. 17A, pp. 1037-49.
3. G. Terlinde, T.W. Duerig, and J.C. Williams: *Metall. Trans. A*, 1983, vol. 14A, pp. 2101-15.
4. C.C. Chen and R.R. Boyer: *JOM*, 1979, vol. 31, pp. 33-39.
5. D. Eylon, A. Vassel, Y. Combres, R.R. Boyer, P.J. Bania, and R.W. Schultz: *JOM*, 1994, vol. 46, pp. 14-15.
6. R.R. Boyer: *JOM*, 1980, vol. 32, pp. 61-65.
7. M.H. Campagnac and A. Vassel: *Designing with Titanium*, Proc. Int. Conf., The Institute of Metals, London, 1986, pp. 261-66.
8. T.W. Duerig, J.E. Allison, and J.C. Williams: *Metall. Trans. A*, 1985, vol. 16A, pp. 739-51.
9. T.W. Duerig and J.C. Williams: *Beta Titanium Alloys in the '80s*, Proc. Symp. Sponsored by the Titanium Committee of AIME, R.R. Boyer and H.W. Rosenberg, eds., TMS, Warrendale, PA, pp. 19-67.
10. G.W. Kuhlman: *Microstructure/Property Relationships in Titanium Aluminides and Alloys*, Y.W. Kim and R.R. Boyer, eds., TMS, Warrendale, PA, 1991, pp. 465-91.

11. S. Suresh and R.O. Ritchie: *Metall. Trans. A*, 1982, vol. 13A, pp. 1627-31.
12. S. Suresh and R.O. Ritchie: *Fatigue Crack Growth Threshold Concepts*, Conf. Proc., D. Davidson and S. Suresh, eds., TMS-AIME, Warrendale, PA, 1984, pp. 227-61.
13. P.K. Liaw: *Mechanics of Fatigue Crack Closure*, ASTM STP 982, J.C. Newman, Jr. and W. Elber, eds., ASTM, Philadelphia, PA, 1988, pp. 62-92.
14. W.J. Evans and A.W. Beale: *Forging and Properties of Aerospace Materials*, Proc. Int. Conf. organized by Activity Group Committee 2, The Metals Society, London, 1978, pp. 170-91.
15. R.J. Bucci and P.C. Paris: *J. Mater.*, 1972, vol. 7, pp. 402-09.
16. A. Yuen, S.W. Hopkins, G.R. Leverant, and C.A. Rau: *Metall. Trans. A*, 1974, vol. 5, pp. 1833-42.
17. P.E. Irving and C.J. Beevers: *Metall. Trans. A,* 1974, vol. 5, pp. 391-98.
18. S. Dubey, A.B.O. Soboyejo, and W.O. Soboyejo: *Acta Mater.*, 1997, vol. 45 (7), pp. 2777-87.
19. J.M. Larsen: Ph.D. Thesis, Carnegie Mellon University, Pittsburgh, PA, 1987.
20. G.T. Gray III and G. Lutjering: *Proc. 2nd Int. Conf. Fatigue and Fatigue Thresholds*, C.J. Beevers, ed., EMAS Pub. Inc., West Midlands, U.K., 1984, vol. II pp. 707-16.
21. K. Sadananda and A.K. Vasudevan: *Fracture Mechanics: 25th volume*, ASTM STP 1220, F. Erdogan, ed., ASTM, Philadelphia, PA, 1995, pp. 484-501.
22. *Annual Book of ASTM Standards*, ASTM, Philadelphia, PA, 1993, vol. 03.01, sec. 3, pp. 679-706.
23. *Quantitative Microscopy*, R.T. DeHoff and F.N. Rhines, eds., McGraw-Hill Book Company, New York, NY, 1968, pp. 45-73 and 77-123.
24. Y. Ohmori, H. Natsui, K. Nakai, and H. Ohtsubo: *Mater. Trans., JIM*, 1998, vol. 39 (1), pp. 40-48.
25. R.O. Ritchie: *Int. Met. Rev.*, 1979, vol. 24, pp. 205-30.
26. P.E. Bretz, J.I. Petit, and A.K. Vasudevan: *Fatigue Crack Growth Threshold Concepts*, D. Davidson and S. Suresh, eds., TMS-AIME, Warrendale, PA, 1984, pp. 163-83.
27. G.W. Kuhlman, A.K. Chakrabarti, T.L. Yu, R. Pishko, and G. Terlinde: in *Microstructure, Fracture Toughness and Fatigue Crack Growth Rate in Titanium Alloys*, A.K. Chakrabarti and J.C. Chesnutt, eds., TMS. AIME, Warrendale, PA, 1987, pp. 171-91.
28. S. Suresh: *Metall. Trans. A*, 1983, vol. 14A, pp. 2375-85.
29. K. Minakawa and J. McEvily: *Scripta Metall.*, 1981, vol. 15, pp. 633-36.
30. K.S. Ravichandran: *Int. J. Fract.*, 1990, vol. 44, pp. 97-110.
31. B.S. Hickman: *Trans. TMS-AIME*, 1969, vol. 245, pp. 1329-36.
32. T.W. Duerig, G.T. Terlinde, and J.C. Williams: *Metall. Trans. A*, 1980, vol. 11A, pp. 1987-98.
33. M. Niinomi and T. Kobayashi: *Iron Steel Inst. Jpn. Int.*, 1991, vol. 31, pp. 848-55.
34. D. DeFontaine, N.E. Paton, and J.C. Williams: *Acta Metall.*, 1971, vol. 19, pp. 1153-62.
35. J.C. Williams, D. De Fontaine, and N.E. Paton: *Metall. Trans.*, 1973, vol. 4, pp. 2701-08.
36. B.S. Hickman: *J. Mater. Sci.*, 1969, vol. 4, pp. 554-63.
37. G.R. Yoder, L.A. Cooley, and T.W. Crooker: *Metall. Trans. A*, 1977, vol. 8A, pp. 1737-43.